Acta Cryst. (1984). A**40**, 152–160

The Resolution Function of Triple-Axis Neutron Spectrometers in the Limit of Small Scattering Angles

BY P. W. MITCHELL, R. A. COWLEY AND S. A. HIGGINS

Department of Physics, University of Edinburgh, Mayfield Road, Edinburgh EH9 3JZ, Scotland

(*Received* 16 *May* 1983; *accepted* 26 *September* 1983)

Abstract

The Cooper–Nathans formulation of the resolution function of a triple-axis crystal spectrometer for neutron-scattering experiments gives a singular resolution matrix when the scattering angle is small. The origin of this singularity is discussed and an alternative derivation of the resolution matrix given which avoids this difficulty. The results are illustrated by numerical calculations for several typical experiments showing that resolution corrections may be large and very significant for experiments at small scattering angles.

1. Introduction

A knowledge of the effects of the experimental resolution in momentum and energy transfer is an important part of any inelastic neutron-scattering experiment. A general formulation of the resolution function of a triple-axis spectrometer was derived by Cooper & Nathans (1967), and discussed by Bjerrum Møller & Nielsen (1970), using a Gaussian approximation for all the contributing transmission functions and crystal mosaic distributions, and the normalisation of this function has been treated at length by Dorner (1972), and Chesser & Axe (1973). Computer programs are widely available for the calculation of this function, and it is known to provide a good representation of the instrumental resolution in many types of triple-axis measurement.

This paper is concerned with one particular limit of the triple-axis resolution function, that of small scattering angle at the sample (small $2\theta_s$ in Fig. 1). Experiments performed at small scattering angles tend to suffer from high background counting rates, and severe restrictions imposed on the energy transfers available by the conservation of momentum requirement (kinematic limits). In the measurement of low-energy magnetic excitations, however, particularly in ferromagnetic materials, such experiments have a number of advantages. Firstly, the magnetic form factor takes its maximum value near (0 0 0), the forward direction. Secondly, scattering from phonons is generally of low intensity, because of the $|\mathbf{Q}|^2$ factor ($\mathbf{Q}$ is the neutron wavevector transfer) in the phonon cross section. Thirdly, the effective resolution near (0 0 0) does not suffer from transverse or longitudinal broadening due to crystal mosaic spreads or lattice-parameter distributions [for the effect of the former on resolution, see Werner & Pynn (1971)], and this allows, under some circumstances, the direct measurement of the magnetic excitations in powdered or polycrystalline materials [*e.g.* Passell, Dietrich & Als-Nielsen (1976), on EuO and EuS] and even amorphous ferromagnetic materials (*e.g.* Axe, Shirane, Mizoguchi & Yamauchi, 1977). For these reasons, many experiments have been performed at small scattering angles in weakly ferromagnetic materials, for which the magnetic scattering may generally be weak compared with the phonon scattering, and large crystals may be difficult to grow.

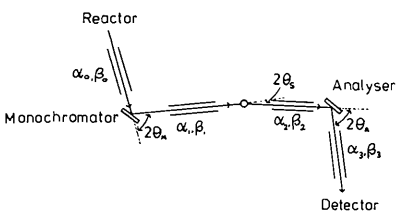

Fig. 1. Plan view of three-axis spectrometer. α, β are horizontal, vertical collimations. ε_M, ε_S, ε_A take the values -1, $+1$ according as scattering at monochromator, sample, analyser is to the right, left. Configuration shown is $\varepsilon_M = +1$, $\varepsilon_S = -1$, $\varepsilon_A = -1$.

As the scattering angle tends to zero, both the efficiency factor and some elements of the resolution matrix diverge, since both contain terms in the reciprocal of the sine of the scattering angle, and extreme care is required to treat the limit correctly. The problem first became apparent to the authors when using a standard computer program to calculate the Cooper–Nathans function at small scattering angles (0·5–1·5°). The resolution matrix itself becomes singular in the limit of the scattering angle tending to zero, and numerical integration over the resolution matrix does not give reliable results unless performed with great care and a high degree of numerical precision.

In the following section, we discuss this limit in the Cooper–Nathans formalism, and then in § 3 we give a more direct formulation of the resolution function, which completely eliminates the problems associated with the Cooper–Nathans function. The results are illustrated by some applications in § 4.

0108-7673/84/020152-09$01.50

2. Small-angle limit of the Cooper–Nathans resolution function

A triple-axis spectrometer (Fig. 1) uses Bragg reflection from a monochromator crystal to define a nominal incident neutron wavevector, $\mathbf{k}_I$,

$$|\mathbf{k}_I| = \frac{\pi}{d_M \sin\theta_M} \tag{2.1}$$

and reflection from an analyser crystal to define a nominal scattered wavevector, $\mathbf{k}_F$,

$$|\mathbf{k}_F| = \frac{\pi}{d_A \sin\theta_A}, \tag{2.2}$$

where $d_{M,A}$ is the appropriate plane spacing and $\theta_{M,A}$ is the appropriate Bragg angle. The directions of incident and scattered beams are defined by the collimators before and after the sample, and the scattered intensity is measured as a function of nominal momentum transfer, $\mathbf{Q}_0$, and nominal energy transfer, $h\nu_0$, where

$$\mathbf{Q}_0 = \mathbf{k}_I - \mathbf{k}_F, \tag{2.3}$$

$$h\nu_0 = \frac{\hbar^2}{2m}(|\mathbf{k}_I|^2 - |\mathbf{k}_F|^2). \tag{2.4}$$

Because of the non-zero angular divergences of the collimators and the mosaic spreads of the monochromator and analyser crystals, neutrons are counted in the detector which have not suffered the nominal momentum and energy changes. The actual changes, $\mathbf{Q}$ and $h\nu$, are related to $\mathbf{Q}_0$ and $h\nu_0$ by

$$\mathbf{Q} = \mathbf{Q}_0 + \boldsymbol{\delta}\mathbf{Q} \tag{2.5}$$

$$h\nu = h\nu_0 + \delta(h\nu). \tag{2.6}$$

It is convenient to write these deviations from the nominal as a four-component vector, $\mathbf{X}$,

$$\mathbf{X} = [\boldsymbol{\delta}\mathbf{Q}, \delta(h\nu)]. \tag{2.7}$$

Cooper & Nathans (1967) showed that the instrumental resolution can be written in the Gaussian approximation as

$$R(\mathbf{X}) = R_0 \exp\{-\tfrac{1}{2}\mathbf{X} \,.\, \mathsf{M} \,.\, \mathbf{X}\}. \tag{2.8}$$

R_0 and M are complicated functions of the angles defined by the collimators, the crystal mosaics and the nominal $|\mathbf{k}_I|$ and $|\mathbf{k}_F|$ (Chesser & Axe, 1973). R_0 also includes terms due to the detector efficiency and the monochromator and analyser reflectivities, and some of the elements of M depend upon the senses of scattering (*i.e.* to the left or to the right) at the monochromator, sample and analyser, in addition to the dependence of both R_0 and M on the scattering angle at the sample.

In detail, R_0 contains the following terms which depend on $2\theta_s$ ($2\theta_s$ is defined in Fig. 1),

$$R_0 \propto \frac{1}{A'^{1/2} \sin 2\theta_s} \tag{2.9}$$

(from Chesser & Axe, equation 6), where A' is as defined by Cooper & Nathans (equation 45*a*) (see also Appendix *A*: *A*.43). In the limit, as $2\theta_s$ goes to zero, the angles between $\mathbf{k}_I$ and $\mathbf{Q}_0$, and between $\mathbf{k}_F$ and $\mathbf{Q}_0$, φ_1 and φ_2, respectively (defined in Fig. 2), tend to the same value, φ, say, since

$$\varphi_1 = \varphi_2 + 2\theta_s \tag{2.10}$$

$$\therefore \quad \varphi_1 \simeq \varphi_2 \equiv \varphi. \tag{2.11}$$

The quantity A' is the sum of six terms, two of which are proportional to

$$\frac{Q_0^2 \cos^2\varphi}{k_F^2 \sin^2 2\theta_s}.$$

For the sake of simplicity, consider two possible cases in whch $2\theta_s$ tends to zero. Firstly, for elastic scattering ($h\nu = 0$, $|\mathbf{k}_I| = |\mathbf{k}_F|$), this quantity decreases as $2\theta_s$ tends to zero ($Q_0 \simeq k_F \sin 2\theta_s$; $\cos^2\varphi \simeq \frac{1}{4}\sin^2 2\theta_s$), A' tends to a constant value and R_0 then diverges as $1/\sin 2\theta_s$. Secondly, for inelastic scattering at constant $\mathbf{Q}_0$, A' behaves like $1/\sin^2 2\theta_s$ as $2\theta_s$ tends to zero, and R_0 tends to a large ($\propto k_F^2/Q_0^2$) constant value.

The behaviour of the elements of the matrix M in the small $2\theta_s$ limit may be illustrated by considering only the in-plane (x and y) components of $\boldsymbol{\delta}\mathbf{Q}$, because the out-of-plane (z) momentum component is de-coupled from the rest and does not depend on $2\theta_s$. For simplicity, we illustrate the results by choosing $\delta(h\nu) = 0$. This gives the section through the resolution function in the x–y plane (the scattering plane) at zero energy deviation. Rotation by an angle, θ, in this plane diagonalizes this part of the matrix (see Appendix *A* for details), and the result is that

$$\theta = -\varepsilon_s \varphi \tag{2.12}$$

$$M'_{xx} \propto \frac{m_{ij}^2}{A' \sin^2 2\theta_s} \tag{2.13}$$

$$M'_{yy} \propto m_{ij}^2, \tag{2.14}$$

where the new x,y axes are related to the Cooper–Nathans axes (parallel, perpendicular to $\mathbf{Q}_0$) by the angle θ, and the m_{ij} are defined in Appendix *A* (equations *A*.6–*A*.13), and are constant as $2\theta_s \to 0$.

Equation (2.12) shows that the rotation, θ, required from the Cooper–Nathans coordinates $\mathbf{X}$ to the eigenvectors of the section of the resolution matrix in the

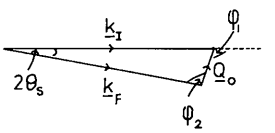

Fig. 2. Scattering triangle (momentum conservation) corresponding to Fig. 1.

scattering plane is just the angle that $\mathbf{Q}_0$ makes with either $\mathbf{k}_I$ or $\mathbf{k}_F$. This means that this section through the resolution function does not change its orientation with respect to $\mathbf{k}_F$, in a constant-**Q** scan, although it rotates with respect to $\mathbf{Q}_0$. Equations (2.13) and (2.14) show that the component of M in the plane and parallel to $\mathbf{k}_F$ is very much larger than the component perpendicular to $\mathbf{k}_F$. This shows that only one of the eigenvalues of M becomes large as $2\theta_s$ becomes small, and that the resolution function is very thin in the direction parallel to $\mathbf{k}_F$ when $\delta(h\nu)=0$.

It should be emphasized that the above is concerned with a particularly simple case of the four-dimensional resolution function, and illustrates the physical effect of the divergence found in the limit of small scattering angle. It suggests that a different approach to the formulation of the resolution function might eliminate the divergence and this is pursued in the next section.

3. Direct formulation for small-angle limit

As may be seen from the results of § 2 above, that component of momentum deviation which is parallel to $\mathbf{k}_F$ is highly correlated with the energy deviation. So, in the small-scattering-angle limit, simplification may be achieved by working in a frame of reference fixed with respect to $\mathbf{k}_F$, say. (Because the scattering angle is small, we could choose $\mathbf{k}_I$ instead, but $\mathbf{Q}_0$ as chosen by Cooper & Nathans varies in direction with respect to $\mathbf{k}_F$ rapidly as $h\nu_0$ is varied.)

The derivation of the resolution function proceeds as for the Cooper–Nathans form to the point where the instrument transmission is expressed in terms of deviations from the nominal $\mathbf{k}_I$ and $\mathbf{k}_F$, in each of three mutually orthogonal directions, in frames fixed with respect to $\mathbf{k}_I$ and $\mathbf{k}_F$, (x parallel to $\mathbf{k}$, and z out of scattering plane in each case). Cooper & Nathans then transform to the four components of **X** and two redundant variables, one in-plane and one out-of-plane, which are then integrated out. In the limit considered here, we take $\mathbf{k}_I$ and $\mathbf{k}_F$ to be parallel (Fig. 3), and transform to three components of $\boldsymbol{\delta\kappa}$ (momentum deviations viewed in the frame fixed with respect to $\mathbf{k}_F$), and three redundant variables, which are integrated out.

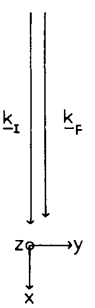

Fig. 3. Coordinates for calculating $\boldsymbol{\kappa}$. Note that, when relating to **Q**, it is still necessary to calculate φ, the angle between $\mathbf{Q}_0$ and $\mathbf{k}_I$ or $\mathbf{k}_F$ (see Fig. 2).

Explicitly, we put

$$\boldsymbol{\delta\kappa} = \boldsymbol{\delta k}_i - \boldsymbol{\delta k}_f \tag{3.1}$$

and transform from the space defined by ($\boldsymbol{\delta k}_i$, $\boldsymbol{\delta k}_f$) to that defined by ($\boldsymbol{\delta k}_i$, $\boldsymbol{\delta\kappa}$). The energy deviation is given by

$$\delta(h\nu) = \frac{\hbar^2}{2m}(2|\mathbf{k}_I|\delta k_{ix} - 2|\mathbf{k}_F|\delta k_{fx}) \tag{3.2}$$

or

$$\delta(h\nu) = \frac{\hbar^2}{m}\left[\frac{(|\mathbf{k}_I|+|\mathbf{k}_F|)}{2}(\delta k_{ix} - \delta k_{fx}) + \frac{(|\mathbf{k}_I|-|\mathbf{k}_F|)}{2}(\delta k_{ix} + \delta k_{fx})\right]. \tag{3.3}$$

At small wavevector transfers, the second term in (3.3) is much smaller than the first, so that the energy deviation is linearly dependent on the x component of $\boldsymbol{\delta\kappa}$,

$$\delta(h\nu) = \frac{\hbar^2}{2m}(|\mathbf{k}_I|+|\mathbf{k}_F|)\,\delta\kappa_x. \tag{3.4}$$

This linear dependence of the energy deviation on one of the momentum-deviation components is the origin of the singularity of the Cooper–Nathans matrix in the limits of small $\mathbf{Q}_0$, and the divergence of the Chesser & Axe efficiency terms. By inserting this dependence analytically at this stage in the derivation, the resulting resolution function, now expressed in terms of three rather than four variables, does not have a singularity as $2\theta_s$ goes to zero.

We now have the resolution matrix M expressed in terms of the three components of κ, one of which (z) is not coupled to the other two. It is straightforward to diagonalize M by a simple rotation in the scattering plane by some angle Θ. All the information about the resolution function is contained in the three eigenvalues of M, the angle Θ, and the efficiency factor R_0, all of which are derived in closed form in Appendix *B*. The energy deviation is given by (3.4). We have therefore eliminated the difficulties encountered at small $2\theta_s$ in the conventional approach.

The expressions derived in Appendix *B* show that the slope of the resolution matrix varies rapidly with energy transfer and in particular that it is possible to focus both energy gain and energy loss at small scattering angles (Axe *et al.*, 1977), as can also be seen qualitatively without the use of algebra. It is possible to obtain further simplifications if the dispersion relation is a function of only $|\mathbf{Q}|$, but these are sufficiently complex, as the resolution function is then no longer Gaussian, that quantitative calculations are just as readily performed with the expressions given in Appendix *B*.

4. Applications of the direct formulation

The prediction of excitation line-widths and line-shapes from model scattering laws may be accomplished very simply in many special cases (Cooper & Nathans, 1967; Haywood, 1971). However, when the scattering law varies rapidly or non-linearly over the volume of the resolution function, such predictions necessarily involve the use of numerical integration methods (Werner & Pynn, 1971; Samuelson, 1971).

A typical ferromagnon dispersion law at small $|\mathbf{Q}|$ may be written as

$$h\nu = \varepsilon_g + D|\mathbf{Q}|^2, \tag{4.1}$$

where ε_g is the anisotropy gap, and is usually very small, and D is called the spin wave stiffness. Thus the excitation energy is a rapidly varying function of $|\mathbf{Q}|$ and, because of the population term in the cross section, the intensity of scattering is a function of $|\mathbf{Q}|$. The problem is further accentuated by the design of triple-axis spectrometers, which usually use relaxed out-of-plane collimation to maximize the scattering intensity, but in an experiment where the nominal wavevector transfer, $\mathbf{Q}_0$, is small, the out-of-plane deviations, δQ_z, may be as large as, or larger than, $|\mathbf{Q}_0|$. Since

$$|\mathbf{Q}|^2 = |\mathbf{Q}_0|^2 + (\delta Q_z)^2 + (\delta Q_y)^2 + (\delta Q_x)^2 + 2|\mathbf{Q}_0|\,\delta Q_x, \tag{4.2}$$

the spin wave energies sampled in the resolution volume may be up to several times as large as the spin wave energy at the nominal wavevector. This means that the scattering observed in a constant-Q scan is broad in energy, and the peak of the scattering may be at some energy higher than the energy of the spin wave at the nominal wavevector. These effects are just the same as those observed for excitations near Bragg peaks at scattering angles other than zero (Samuelsen, Hutchings & Shirane, 1970; Hutchings, Als-Nielsen, Lingard & Walker, 1981). It is not difficult to show that, if the in-plane resolution were to be perfectly sharp, the scattering from spin waves in a constant-Q scan would appear as in Fig. 4. The intensity, $I(\nu)$, is given by

$$I(\nu) = \begin{cases} [n(\nu) + \frac{1}{2} \pm \frac{1}{2}] \exp\left\{-\frac{1}{2}M_{zz}\left[\dfrac{|h\nu| - \varepsilon_g}{D} - Q_0^2\right]\right\} \\ \qquad \text{if } |h\nu| \geq \varepsilon_g + DQ_0^2 \\ 0 \qquad \text{otherwise,} \end{cases} \tag{4.3}$$

where $+$, $-$ apply for neutron energy loss, gain and $n(\nu)$ is the Bose–Einstein population factor. That such scattering in practice never takes this form indicates that the in-plane resolution must also be considered, with the effect of rounding the sharp edge at low frequencies, and moving the maximum intensity to higher frequency.

The most satisfactory method of accounting for resolution effects in this case is to use a computer program to generate intensities by integrating an assumed dispersion relation over the calculated resolution function. This has been done, using the direct formulation of § 3, for a number of different data sets, taken under different conditions in small-scattering-angle experiments. Use of this method avoids the difficulties associated with the use of the Cooper–Nathans formulation mentioned in the *Introduction*. Firstly, the resolution matrix is known exactly in diagonal form, and so the problems either of trying to integrate over a sharp function in the crystal coordinates, or of trying to diagonlize a nearly singular matrix to transform to the natural resolution-function coordinates, are avoided. Secondly, the number of dimensions of the numerical integral is reduced by one, enabling a more accurate integral evaluation for a given amount of computing resources.

Fig. 5 shows spin wave scattering intensities generated by numerical integration from the form derived in Appendix *B* (equation *B*.13) utilizing the directly derived resolution matrix (equations *B*.4–*B*.9) and assuming a gapless quadratic spin wave dispersion relation. The figure shows the effects of changing spectrometer configuration and vertical collimation.

Fig. 6 illustrates simulated intensities fitted by non-linear regression analysis to some of the data of Bernhoeft, Lonzarich, Mitchell & Paul (1983) for Ni_3Al. The function form is defined by a flat background term, a Gaussian peak to represent elastic scattering, and the intensity due to spin wave scattering (dispersion defined by equation 4.1). This last term was simulated by performing a numerical integration over the resolution function, as derived in § 3, of a δ-function spin wave scattering law. The importance of an accurate resolution correction for this data becomes clear from the effective shift of the nominal peak frequency by up to ~33%, and an

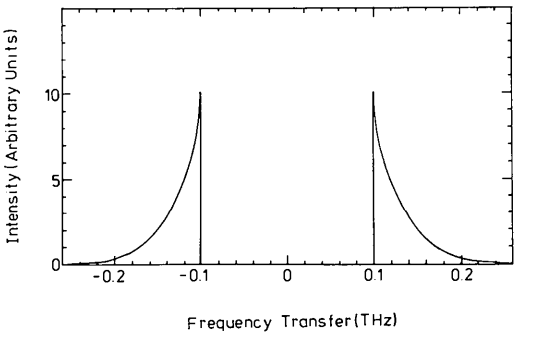

Fig. 4. Intensity of scattering from spin waves which would be observed in a constant-**Q** scan if the only resolution contribution were the out-of-plane momentum component. Calculations were made using equation (4.3) in the high-temperature limit, so that $n(\nu) + \frac{1}{2} \pm \frac{1}{2} \rightarrow k_B T/h\nu$. Values of parameters used were $M_{zz} = 500$ Å^2, $Q_0 = 0{\cdot}1$ Å^{-1}, $\varepsilon_g = 0$ and $D = 10$ THz Å^2.

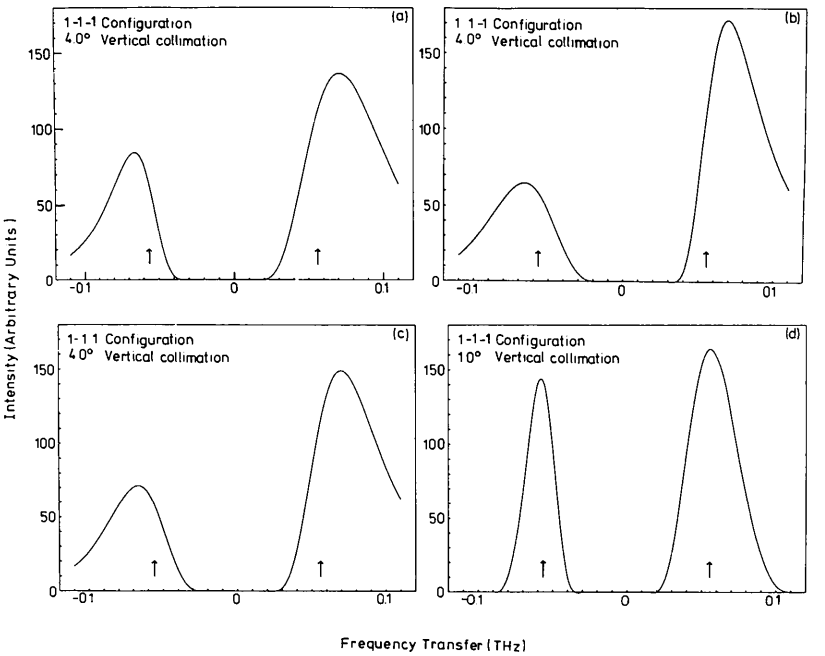

Fig. 5. Pure spin wave scattering generated by the computer program. (*a*), (*b*) and (*c*) differ only in configuration of the spectrometer with the vertical collimation the same for each, namely $\beta_0 = \beta_1 = \beta_2 = \beta_3 = 4{\cdot}0°$. (*a*) and (*d*) differ in vertical collimation, but have the same configuration [the intensity shown for (*d*) has been amplified by a factor of eight]. Note that arrows point to the nominal spin wave energy. In each, $Q = 0{\cdot}075$ Å^{-1}, $\varepsilon_g = 0$ and $D = 10$ THz Å^2. Horizontal collimation is (*a*) 30′, (*b*) 20′, (*c*) 20′, (*d*) 30′. $k_F = 1{\cdot}55$ Å^{-1}, $2\theta_s \leq 2{\cdot}8°$.

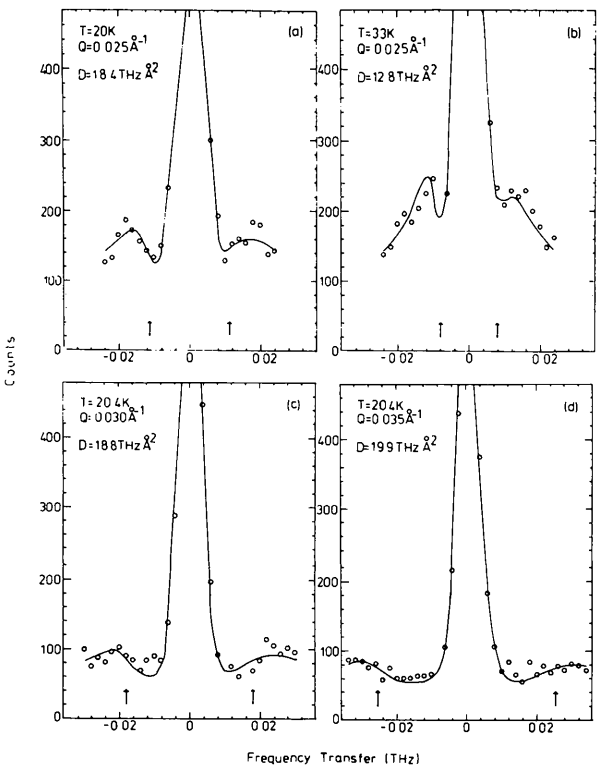

Fig. 6. Experimental data (O) and computer-generated least-squares fit (solid line) showing spin wave scattering from Ni_3Al at various wavevector transfers and temperatures ($T_c \simeq 40$ K). $2\theta_s \leq 1{\cdot}3$, $1{\cdot}6$, $1{\cdot}8°$ for (*a*) and (*b*), (*c*), (*d*), respectively. $k_F = 1{\cdot}1$ Å^{-1}. See text for details.

energy width in the spin wave peak generated by resolution effects which is comparable to the observed peak frequency, and roughly double the energy width observed for **Q**-independent elastic scattering.

5. Conclusions

We have investigated the Cooper–Nathans resolution function for triple-axis neutron spectrometers in the limit of small scattering angles and found that two of the four deviations from the nominal wavevector (three components) and from the nominal energy become linearly dependent, giving rise to a singular resolution matrix and efficiency factor.

By treating this dependence analytically we have derived a resolution function for the small-scattering-angle limit which is simpler and both easier and faster to compute than the general Cooper–Nathans function. Numerical simulation techniques have been employed which show that this direct formulation allows a detailed analysis of data from small-angle experiments.

We emphasise that the use of standard Cooper–Nathans programs for the calculation of the resolution effects does not give satisfactory results for small scattering angles, unless the resolution matrix is diagonalized and the numerical integrations performed in the diagonlized frame of reference and unless a high degree of numerical precision is used to cope with the singularity of the matrix. The direct

analysis we have given allows the calculations to be performed more accurately and more speedily.

This work was supported by the SERC.

APPENDIX A
Details of Cooper–Nathans at small angles

In the Gaussian approximation, the resolution function may be written

$$R = R_0(\mathbf{X}) \exp\{-\tfrac{1}{2}\mathbf{X} \,.\, \mathsf{M}(\mathbf{X}) \,.\, \mathbf{X}\}, \qquad (A.1)$$

where $\mathbf{X}$ is the space defined by a set of deviations from nominal parameters, $R_0(\mathbf{X})$ is the efficiency factor, and $\mathsf{M}(\mathbf{X})$ is the resolution matrix in the space $\mathbf{X}$.

The Cooper–Nathans function is expressed with

$$\mathbf{X} = [\delta\mathbf{Q}, \delta(h\nu)], \qquad (A.2)$$

where the axes of $\delta\mathbf{Q}$ are fixed with respect to $\mathbf{Q}_0$.

In the space defined by

$$\mathbf{X} = (\delta\mathbf{k}_i, \delta\mathbf{k}_f), \qquad (A.3)$$

where

$$\delta\mathbf{k}_j = \delta k_{jx}, \delta k_{jy}, \delta k_{jz}, \qquad (A.4)$$

the resolution matrix is

$$\mathsf{M}(\delta\mathbf{k}_i, \delta\mathbf{k}_f) = \begin{pmatrix} m_{11} & m_{12} & 0 & 0 & 0 & 0 \\ m_{12} & m_{22} & 0 & 0 & 0 & 0 \\ 0 & 0 & m_{33} & 0 & 0 & 0 \\ 0 & 0 & 0 & m_{44} & m_{45} & 0 \\ 0 & 0 & 0 & m_{45} & m_{55} & 0 \\ 0 & 0 & 0 & 0 & 0 & m_{66} \end{pmatrix}, \qquad (A.5)$$

where

$$m_{11} = (2\tan\theta_M)^2\left(\frac{1}{\alpha_0^2}+\frac{1}{(2\eta_M)^2}\right)\frac{1}{k_I^2} = b_5 \qquad (A.6)$$

$$m_{12} = -2\varepsilon_M \tan\theta_M\left(\frac{1}{\alpha_0^2}+\frac{1}{2\eta_M^2}\right)\frac{1}{k_I^2} = -\varepsilon_M b_0 \qquad (A.7)$$

$$m_{22} = \left(\frac{1}{\alpha_0^2}+\frac{1}{\alpha_1^2}+\frac{1}{\eta_M^2}\right)\frac{1}{k_I^2} = b_1 \qquad (A.8)$$

$$m_{33} = \left(\frac{1}{\beta_1^2}+\frac{1}{(2\sin\theta_M\eta'_M)^2+\beta_0^2}\right)\frac{1}{k_I^2} = a_{11}^2 \qquad (A.9)$$

$$m_{44} = (2\tan\theta_A)^2\left(\frac{1}{\alpha_3^2}+\frac{1}{(2\eta_A)^2}\right)\frac{1}{k_F^2} = b_3 \qquad (A.10)$$

$$m_{45} = 2\varepsilon_A \tan\theta_A\left(\frac{1}{\alpha_3^2}+\frac{1}{2\eta_A^2}\right)\frac{1}{k_F^2} = -\varepsilon_A b_4 \qquad (A.11)$$

$$m_{55} = \left(\frac{1}{\alpha_3^2}+\frac{1}{\alpha_2^2}+\frac{1}{\eta_A^2}\right)\frac{1}{k_F^2} = b_2 \qquad (A.12)$$

$$m_{66} = \left(\frac{1}{\beta_2^2}+\frac{1}{(2\sin\theta_A\eta'_A)^2+\beta_3^2}\right)\frac{1}{k_F^2} = a_{12}^2, \qquad (A.13)$$

where the θ's, ε's, α's and β's are defined in Fig. 1, $\mathbf{k}_I$ and $\mathbf{k}_F$ are defined by (2.1) and (2.2), $\eta_{M,A}$, $\eta'_{M,A}$ are the horizontal and vertical mosaics of monochromator and analyser, and the b's and a's are those defined by Cooper & Nathans (1967), equations (44) and (55) (note the correction given by Dorner, 1972).

The transformation to the space $\mathbf{x}'$, where

$$\mathbf{x}' = [\delta\mathbf{Q}, \delta(h\nu), \delta k_{ix}, \delta k_{iz}], \qquad (A.14)$$

is given by the matrix U, so that

$$\mathbf{x}' = \mathsf{U} \,.\, \mathbf{X}. \qquad (A.15)$$

If the inverse of U is V, then

$$\mathsf{V} = \begin{pmatrix} 0 & 0 & 0 & 0 & v_{15} & 0 \\ v_{21} & v_{22} & 0 & v_{24} & v_{25} & 0 \\ 0 & 0 & 0 & 0 & 0 & v_{36} \\ 0 & 0 & 0 & v_{44} & v_{45} & 0 \\ v_{51} & v_{52} & 0 & v_{54} & v_{55} & 0 \\ 0 & 0 & v_{63} & 0 & 0 & v_{66} \end{pmatrix}, \qquad (A.16)$$

where

$$v_{15} = 1 \qquad (A.17)$$

$$v_{21} = -\varepsilon_s \cos\varphi_2/\sin 2\theta_s \qquad (A.18)$$

$$v_{22} = \sin\varphi_2/\sin 2\theta_s \qquad (A.19)$$

$$v_{24} = -\varepsilon_s/(\gamma \sin 2\theta_s) \qquad (A.20)$$

$$v_{25} = -\varepsilon_s(\cos 2\theta_s - k_I/k_F)/\sin 2\theta_s \qquad (A.21)$$

$$= -\varepsilon_s Q_0 \cos\varphi_1/(k_F \sin 2\theta_s) \qquad (A.22)$$

$$v_{36} = 1 \qquad (A.23)$$

$$v_{44} = -1/\gamma \qquad (A.24)$$

$$v_{45} = k_I/k_F \qquad (A.25)$$

$$v_{51} = -\varepsilon_s \cos\varphi_1/\sin 2\theta_s \qquad (A.26)$$

$$v_{52} = \sin\varphi_1/\sin 2\theta_s \qquad (A.27)$$

$$v_{54} = -\varepsilon_s \cos 2\theta_s/(\gamma \sin 2\theta_s) \qquad (A.28)$$

$$v_{55} = -\varepsilon_s[1-(k_I/k_F)\cos 2\theta_s]/\sin 2\theta_s \qquad (A.29)$$

$$= -\varepsilon_s Q_0 \cos\varphi_2/(k_F \sin 2\theta_s) \qquad (A.30)$$

$$v_{63} = 1 \qquad (A.31)$$

$$v_{66} = 1, \qquad (A.32)$$

where φ_1, φ_2 and $2\theta_s$ are defined in Fig. 2, and

$$\gamma = k_F\hbar^2/m. \qquad (A.33)$$

The dependence on δk_{ix}, δk_{iz} is irrelevant, so these parameters are removed by integrating over all possible values. This leaves the Cooper–Nathans matrix, which has four components, one of which, that in δQ_z, is uncoupled from the other three.

Consider only δQ_x, δQ_y, with $\delta(h\nu)$ set to zero;

$$\mathsf{M} = \begin{pmatrix} M_{xx} & M_{xy} \\ M_{xy} & M_{yy} \end{pmatrix}. \qquad (A.34)$$

The elements are

$$M_{xx} = (\rho v_{21}^2 + \sigma v_{51}^2 - 2\tau v_{21} v_{51})/A' \quad (A.35)$$

$$M_{xy} = [\rho v_{21} v_{22} + \sigma v_{51} v_{52} - \tau(v_{21} v_{52} + v_{22} v_{51})]/A' \quad (A.36)$$

$$M_{yy} = (\rho v_{22}^2 + \sigma v_{52}^2 - 2\tau v_{22} v_{52})/A', \quad (A.37)$$

where

$$\rho = m_{22} m_{55} v_{55}^2 + m_{77}^2 v_{15}^2 + m_{22} m_{44} v_{45}^2 + 2 m_{45} m_{22} v_{45} v_{55} \quad (A.38)$$

$$\sigma = m_{22} m_{55} v_{25}^2 + m_{88}^2 v_{45}^2 + m_{55} m_{11} v_{15}^2 + 2 m_{55} m_{12} v_{15} v_{25} \quad (A.39)$$

$$\tau = m_{22} m_{55} v_{25} v_{55} + m_{45} m_{22} v_{45} v_{25} + m_{55} m_{12} v_{15} v_{55} + m_{45} m_{12} v_{45} v_{15} \quad (A.40)$$

with

$$m_{77}^2 = m_{11} m_{22} - m_{12}^2 \quad (A.41)$$

$$m_{88}^2 = m_{44} m_{55} - m_{45}^2 \quad (A.42)$$

and

$$A' = m_{22} v_{25}^2 + m_{44} v_{45}^2 + m_{55} v_{55}^2 + m_{11} v_{15}^2 + 2 m_{12} v_{15} v_{25} + 2 m_{45} v_{55} v_{45}. \quad (A.43)$$

[Compare (*A*.43) with Cooper & Nathans' equation (45*a*).]

Diagonalization by rotation in the x–y plane through an angle θ gives

$$\mathbf{M}' = \begin{pmatrix} M'_{xx} & 0 \\ 0 & M'_{yy} \end{pmatrix} \quad (A.44)$$

with

$$M'_{xx} = \tfrac{1}{2}[\omega + (\chi^2 + \psi^2)^{1/2}] \quad (A.45)$$

$$M'_{yy} = \tfrac{1}{2}[\omega - (\chi^2 + \psi^2)^{1/2}], \quad (A.46)$$

where

$$\omega = [\rho + \sigma - 2\tau \cos(\varphi_1 - \varphi_2)]/A' \sin^2 2\theta_s \quad (A.47)$$

$$\chi = [\rho \cos 2\varphi_2 + \sigma \cos 2\varphi_1 - 2\tau \cos(\varphi_1 + \varphi_2)]/A' \sin^2 2\theta_s \quad (A.48)$$

$$\psi = [\rho \sin 2\varphi_2 + \sigma \sin 2\varphi_1 - 2\tau \sin(\varphi_1 + \varphi_2)]/A' \sin^2 2\theta_s \quad (A.49)$$

and

$$\theta = \tfrac{1}{2} \arctan(-\varepsilon_s \psi/\chi). \quad (A.50)$$

This is an exact result from the Cooper–Nathans matrix. Now, the approxiation of (2.11) gives

$$\theta = -\varepsilon_s \varphi \quad (A.51)$$

$$M'_{xx} = (\rho + \sigma - 2\tau)/A' \sin^2 2\theta_s \quad (A.52)$$

$$M'_{yy} = \xi/(\rho + \sigma - 2\tau), \quad (A.53)$$

where

$$\xi = m_{55} m_{77}^2 v_{15}^2 + m_{22} m_{88}^2 v_{45}^2. \quad (A.54)$$

Note that, although ρ, σ and τ independently contain divergent terms as $2\theta_s \to 0$, the combination $(\rho + \sigma - 2\tau)$ does not diverge but tends to the limit

$$\rho + \sigma - 2\tau \to (m_{22} + m_{55})(m_{11} v_{15}^2 + m_{44} v_{45}^2) - (m_{12} v_{15} + m_{45} v_{45})^2. \quad (A.55)$$

The result (*A*.52) and (*A*.53) indicates that one of the three diagonal elements arising from the δQ_x, δQ_y, $\delta(h\nu)$ terms in $\mathbf{M}$ behaves in the small $2\theta_s$ limit as

$$M_{ll} \propto \frac{1}{A \sin^2 2\theta_s}. \quad (A.56)$$

Dorner (1972) showed that the terms in R_0 which depend on scattering at the sample must be derived from the determinant of the resolution matrix, since

$$R_0 = \frac{V_I V_F}{4\pi^2} |\mathbf{M}|^{1/2} \quad (A.57)$$

(Dorner's equation 22), where V_I and V_F are primary and secondary spectrometer resolution volumes and are independent of scattering geometry at the sample. This is consistent with one diagonal element behaving as in (*A*.56), since $|\mathbf{M}|$ is the product of the diagonal elements, and R_0 behaves as shown in (2.9).

APPENDIX *B*

Resolution matrix and efficiency factor in the direct formulation

The derivation of the resolution function in this form follows that of the Cooper–Nathans form up to the point where the detection probability is expressed in terms of the deviations from the nominal incident and scattered wavevectors (*A*.3–*A*.13). We transform to the three components of $\delta\boldsymbol{\kappa}$ (defined in 3.1) and $\delta\mathbf{k}_i$

$$\mathbf{M}(\delta\mathbf{k}_i, \delta\boldsymbol{\kappa}) = \begin{pmatrix} m_{11}+m_{44} & m_{12}+m_{45} & 0 \\ m_{12}+m_{45} & m_{22}+m_{55} & 0 \\ 0 & 0 & m_{33}+m_{66} \\ -m_{44} & -m_{45} & 0 \\ -m_{45} & -m_{55} & 0 \\ 0 & 0 & -m_{66} \end{pmatrix} \begin{pmatrix} -m_{44} & -m_{45} & 0 \\ -m_{45} & -m_{55} & 0 \\ 0 & 0 & -m_{66} \\ m_{44} & m_{45} & 0 \\ m_{45} & m_{55} & 0 \\ 0 & 0 & m_{66} \end{pmatrix} \quad (B.1)$$

Now integrate over the three components of $\delta\mathbf{k}_i$. This gives

$$\mathbf{M}(\delta\boldsymbol{\kappa})=\begin{pmatrix}(m_{44}m_{77}^2+m_{11}m_{88}^2)/s & (m_{45}m_{77}^2+m_{12}m_{88}^2)/s & 0\\ (m_{45}m_{77}^2+m_{12}m_{88}^2)/s & (m_{55}m_{77}^2+m_{22}m_{88}^2)/s & 0\\ 0 & 0 & m_{33}m_{66}/(m_{33}+m_{66})\end{pmatrix}, \tag{B.2}$$

where

$$s=(m_{22}+m_{55})(m_{11}+m_{44})-(m_{12}+m_{45})^2. \tag{B.3}$$

This matrix is diagonalized by a rotation through Θ in the x–y plane,

$$\mathbf{M}(\delta\boldsymbol{\kappa}')=\begin{pmatrix}\tfrac{1}{2}[\Omega+(X^2+\Psi^2)^{1/2}] & 0 & 0\\ 0 & \tfrac{1}{2}[\Omega-(X^2+\Psi^2)^{1/2}] & 0\\ 0 & 0 & m_{33}m_{66}/(m_{33}+m_{66})\end{pmatrix}, \tag{B.4}$$

where

$$\delta\boldsymbol{\kappa}'=\begin{pmatrix}\cos\Theta & -\sin\Theta & 0\\ \sin\Theta & \cos\Theta & 0\\ 0 & 0 & 1\end{pmatrix}\delta\boldsymbol{\kappa} \tag{B.5}$$

with

$$\Theta=\tfrac{1}{2}\arctan(\Psi/X) \tag{B.6}$$

and

$$\Omega=[(m_{44}+m_{55})m_{77}^2+(m_{11}+m_{22})m_{88}^2]/s \tag{B.7}$$

$$X=[(m_{44}-m_{55})m_{77}^2+(m_{11}-m_{22})m_{88}^2]/s \tag{B.8}$$

$$\Psi=[2m_{45}m_{77}^2+2m_{12}m_{88}^2]/s. \tag{B.9}$$

In order to derive the pre-exponential term in the resolution function, it is necessary to include the factors which arise from the elimination of $\delta\mathbf{k}_i$. To avoid ambiguity, the efficiency factor will be expressed in terms of the ratio of the detector counting rate, Φ_D, to the flux per unit solid angle per unit wavevector from the reactor, $\varphi(k_I)$,

$$\begin{aligned}\frac{\Phi_D}{\varphi(k_I)}=&E_D(k_F)\frac{2\pi\hbar}{m}p_M(k_I)p_A(k_I)\frac{1}{k_I^3}\\ &\times\left[1+\left(\frac{2\eta'_M\sin\theta_M}{\beta_0}\right)^2\right]^{-1/2}\\ &\times\left[1+\left(\frac{2\eta'_A\sin\theta_A}{\beta_3}\right)^2\right]^{-1/2}\\ &\times(m_{33}+m_{66})^{-1/2}s^{-1/2}\\ &\times\iiiint S(\mathbf{Q},\nu)\exp\{-\tfrac{1}{2}\delta\boldsymbol{\kappa}'\mathbf{M}(\delta\boldsymbol{\kappa}')\delta\boldsymbol{\kappa}'\}\\ &\times\delta\left(\delta\nu-\frac{\hbar}{4\pi m}(|\mathbf{k}_I|+|\mathbf{k}_F|)\delta\kappa_x\right)\mathrm{d}\nu\,\mathrm{d}(\delta\boldsymbol{\kappa}'),\end{aligned} \tag{B.10}$$

where $E_D(k_F)$ is the detector efficiency at k_F, $p_{M,A}(k_I, k_F)$ is the peak reflectivity of monochromator or analyser at the appropriate wavevector, and other symbols are defined above.

In the same way, we may write the total flux incident on the sample, Φ_s,

$$\begin{aligned}\frac{\Phi_S}{\varphi(k_I)}=&(2\pi)^{3/2}p_M(k_I)k_I\cot\theta_M\\ &\times\left[1+\left(\frac{2\eta'_M\sin\theta_M}{\beta_0}\right)^2\right]^{-1/2}\\ &\times\left[\frac{1}{\beta_1^2}+\frac{1}{\beta_0^2+(2\eta'_M\sin\theta_M)^2}\right]^{-1/2}\\ &\times\left[\frac{1}{\alpha_0^2\alpha_1^2}+\frac{1}{\alpha_0^2(2\eta_M)^2}+\frac{1}{\alpha_1^2(2\eta_M)^2}\right]^{-1/2}.\end{aligned} \tag{B.11}$$

Under certain circumstances, it may be desirable to move the fission-chamber monitor, which is usually used to measure the flux incident on the sample, away from the sample to before the monochromator-to-sample collimator, to cut down the background due to small-angle scattering from the monitor. In this case, denote the horizontal, vertical collimation from monochromator to monitor by α_5, β_5. The counting rate of the monitor, Φ_M, is then given by

$$\begin{aligned}\frac{\Phi_M}{\varphi(k_I)}=&\frac{E_M}{k_I}(2\pi)^{3/2}p_M(k_I)k_I\cot\theta_M\\ &\times\left[1+\left(\frac{2\eta'_M\sin\theta_M}{\beta_0}\right)^2\right]^{-1/2}\\ &\times\left[\frac{1}{\beta_5^2}+\frac{1}{\beta_0^2+(2\eta'_M\sin\theta_M)^2}\right]^{-1/2}\\ &\times\left[\frac{1}{\alpha_0^2\alpha_5^2}+\frac{1}{\alpha_0^2(2\eta_M)^2}+\frac{1}{\alpha_5^2(2\eta_M)^2}\right]^{-1/2},\end{aligned} \tag{B.12}$$

where E_M is the monitor efficiency at $K_I=1$, and the efficiency is assumed to be proportional to $(k_I)^{-1}$.

The experimentally measured quantity is Φ_D/Φ_M,

$$\frac{\Phi_D}{\Phi_M}=\frac{E_D(k_F)}{E_M}\frac{\hbar}{\sqrt{2\pi m}}\frac{p_A(k_F)}{k_I^3\cot\theta_M}\times\left[1+\left(\frac{2\eta'_A\sin\theta_A}{\beta_3}\right)^2\right]^{-1/2}\times\left[\frac{1}{\beta_5^2}+\frac{1}{\beta_0^2+(2\eta'_M\sin\theta_M)^2}\right]^{1/2}\times\left[\frac{1}{\alpha_0^2\alpha_5^2}+\frac{1}{\alpha_0^2(2\eta_M)^2}+\frac{1}{\alpha_5^2(2\eta_M)^2}\right]^{1/2}\times(m_{33}+m_{66})^{-1/2}s^{-1/2}\iiiint S(\mathbf{Q},\nu)\times\exp\{-\tfrac{1}{2}\boldsymbol{\delta\kappa}'\mathbf{M}(\boldsymbol{\delta\kappa}')\boldsymbol{\delta\kappa}'\}\times\delta\left[\delta\nu-\frac{\hbar}{4\pi m}(|\mathbf{k}_I|+|\mathbf{k}_F|)\delta\kappa_x\right]\mathrm{d}\nu\,\mathrm{d}(\boldsymbol{\delta\kappa}'). \tag{B.13}$$

The integral involves three different ways of expressing the deviations from the nominal wavevector transfer (and so, by equation 3.4, from the nominal energy transfer). They are related by (*B*.5) and the following:

$$\boldsymbol{\delta Q}=\begin{pmatrix}\cos\varphi & -\varepsilon_s\sin\varphi & 0\\ \varepsilon_s\sin\varphi & \cos\varphi & 0\\ 0 & 0 & 1\end{pmatrix}\boldsymbol{\delta\kappa} \tag{B.14}$$

or

$$\boldsymbol{\delta Q}=\begin{pmatrix}\cos(\Theta-\varepsilon_s\varphi) & \sin(\Theta-\varepsilon_s\varphi) & 0\\ -\sin(\Theta-\varepsilon_s\varphi) & \cos(\Theta-\varepsilon_s\varphi) & 0\\ 0 & 0 & 1\end{pmatrix}\boldsymbol{\delta\kappa}'. \tag{B.15}$$

The effects of sample mosaic have not been incorporated into the resolution function here because, in the limit of small scattering angles, the three-dimensional ferromagnetic systems considered here show isotropic spin wave scattering (equation 4.1). Thus mosaic effects are unimportant, even in powdered or polycrystalline samples. For systems which display anisotropic scattering at small angles, mosaic effects could be incorporated into the transverse momentum components of the resolution function by performing the transformation (*B*.14) on the matrix (*B*.2) and including the terms given by Werner & Pynn (1971).

Note that the spectrometer focusing may be optimized (R_0 maximized) by making s smaller by suitable choice of configuration. In the small $2\theta_s$ limit, this may be achieved with $\varepsilon_A=-\varepsilon_M$.

References

AXE, J. D., SHIRANE, G., MIZOGUCHI, T. & YAMAUCHI, K. (1977). *Phys. Rev. B*, **15**, 2763–2770.

BERNHOEFT, N. R., LONZARICH, G. G., MITCHELL, P. W. & PAUL, D. MCK. (1983). *Phys. Rev. B*, **28**, 422–424.

BJERRUM MØLLER, H. & NEILSEN, M. (1970). *Instrumentation for Neutron Inelastic Scattering Research*, pp. 49–70. Vienna: IAEA.

CHESSER, N. J. & AXE, J. D. (1973). *Acta Cryst.* A**29**, 160–169.

COOPER, M. J. & NATHANS, R. (1967). *Acta Cryst.* **23**, 357–367.

DORNER, B. (1972). *Acta Cryst.* A**28**, 319–327.

HAYWOOD, B. C. (1971). *Acta Cryst.* A**27**, 408–410.

HUTCHINGS, M. T., ALS-NIELSEN, J., LINGARD, P. A. & WALKER, P. J. (1981). *J. Phys. C*, **14**, 5327–5345.

PASSELL, L., DIETRICH, O. W. & ALS-NIELSEN, J. (1976). *Phys. Rev. B*, **14**, 4897–4907.

SAMUELSEN, E. J. (1971). In *Structural Phase Transitions and Soft Modes*; edited by E. J. SAMUELSON, E. ANDERSEN & J. FEDER, pp. 189–215, Oslo: Universitetsforlaget Trykningssentral.

SAMUELSEN, E. J., HUTCHINGS, M. T. & SHIRANE, G. (1970). *Physica (Utrecht)*, **48**, 13–42.

WERNER, S. A. & PYNN, R. (1971). *J. Appl. Phys.* **42**, 4736–4749.